Remodeling of T-Tubules and Reduced Synchrony of Ca^{2+} Release in Myocytes From Chronically Ischemic Myocardium

Frank R. Heinzel, Virginie Bito, Liesbeth Biesmans, Ming Wu, Elke Detre, Frederik von Wegner, Piet Claus, Steven Dymarkowski, Frederik Maes, Jan Bogaert, Frank Rademakers, Jan D'hooge, Karin Sipido

Abstract—In ventricular cardiac myocytes, T-tubule density is an important determinant of the synchrony of sarcoplasmic reticulum (SR) Ca^{2+} release and could be involved in the reduced SR Ca^{2+} release in ischemic cardiomyopathy. We therefore investigated T-tubule density and properties of SR Ca^{2+} release in pigs, 6 weeks after inducing severe stenosis of the circumflex coronary artery (91±3%, N=13) with myocardial infarction (8.8±2.0% of total left ventricular mass). Severe dysfunction in the infarct and adjacent myocardium was documented by magnetic resonance and Doppler myocardial velocity imaging. Myocytes isolated from the adjacent myocardium were compared with myocytes from the same region in weight-matched control pigs. T-tubule density quantified from the di-8-ANEPPS (di-8-butyl-amino-naphthyl-ethylene-pyridinium-propyl-sulfonate) sarcolemmal staining was decreased by 27±7% ($P<0.05$). Synchrony of SR Ca^{2+} release (confocal line scan images during whole-cell voltage clamp) was reduced in myocardium myocytes. Delayed release (ie, half-maximal $[Ca^{2+}]_i$ occurring later than 20 ms) occurred at 35.5±6.4% of the scan line in myocardial infarction versus 22.7±2.5% in control pigs ($P<0.05$), prolonging the time to peak of the line-averaged $[Ca^{2+}]_i$ transient (121±9 versus 102±5 ms in control pigs, $P<0.05$). Delayed release colocalized with regions of T-tubule rarefaction and could not be suppressed by activation of protein kinase A. The whole-cell averaged $[Ca^{2+}]_i$ transient amplitude was reduced, whereas L-type Ca^{2+} current density was unchanged and SR content was increased, indicating a reduction in the gain of Ca^{2+}-induced Ca^{2+} release. In conclusion, reduced T-tubule density during ischemic remodeling is associated with reduced synchrony of Ca^{2+} release and reduced efficiency of coupling Ca^{2+} influx to Ca^{2+} release. **(*Circ Res*. 2008;102:338-346.)**

Key Words: myocardial infarction ■ contractility ■ myocytes ■ calcium

Although new therapeutic approaches have decreased the mortality associated with myocardial infarction (MI) over the past decades,[1] many patients nevertheless sustain a regional loss of myocardial contractile tissue following an ischemic event. The resulting increased hemodynamic burden on the left ventricle leads to structural and functional changes in the remaining viable myocardium, which further reduces ventricular performance, a process referred to as myocardial remodeling.[2] Sustained regional chronic and/or intermittent ischemia further contributes to this process, and the resulting ischemic cardiomyopathy is currently among the major causes of heart failure.[3]

Contractile dysfunction of the ventricle is partly related to the abnormal loading in vivo[4] and partly to the intrinsic properties of the cardiomyocytes. Myocytes isolated from patients with ischemic cardiomyopathy at the time of heart transplantation have a reduced contractile function resulting from abnormal Ca^{2+} handling.[5–7] Animal models have examined the mechanisms of cellular dysfunction in ischemic cardiomyopathy in more detail. Myocytes from the infarct border zone have a reduced contraction and slowed and reduced $[Ca^{2+}]_i$ transients.[8–11] The mechanisms leading to this impaired Ca^{2+} handling are not completely understood. Decreased intracellular Ca^{2+} release may be the result of a reduced sarcoplasmic reticulum (SR) Ca^{2+} content caused by decreased SR Ca^{2+} pump activity, as has been observed in some[8,11,12] but not all[10,13] models of postinfarct remodeling. Increased Na/Ca exchange (NCX) activity and abnormal expression and phosphorylation of the ryanodine receptor (RyR) have also been reported.[10,14,15]

Original received March 30, 2006; resubmission received July 19, 2007; revised resubmission received November 1, 2007; accepted November 29, 2007.

From the Division of Experimental Cardiology (F.R.H., V.B., L.B., E.D., K.S.), Division of Cardiac Imaging (M.W., P.C., F.R., J.D'h.), Division of Radiology (S.D., J.B.), Department of Electrical Engineering (F.M.), University Hospital Gasthuisberg and University of Leuven, Belgium; and Medical Biophysics (F.v.W.), Institute for Physiology and Pathophysiology, University of Heidelberg, Germany. F.R.H. is currently at the Division of Cardiology, Medical University of Graz, Austria.

Correspondence to Karin R. Sipido, MD, PhD, Laboratory of Experimental Cardiology, KUL, Campus Gasthuisberg O/N 7th Floor, Herestraat 49, B-3000 Leuven, Belgium. E-mail Karin.Sipido@med.kuleuven.ac.be

Circulation Research **is available at http://circres.ahajournals.org** **DOI: 10.1161/CIRCRESAHA.107.160085**

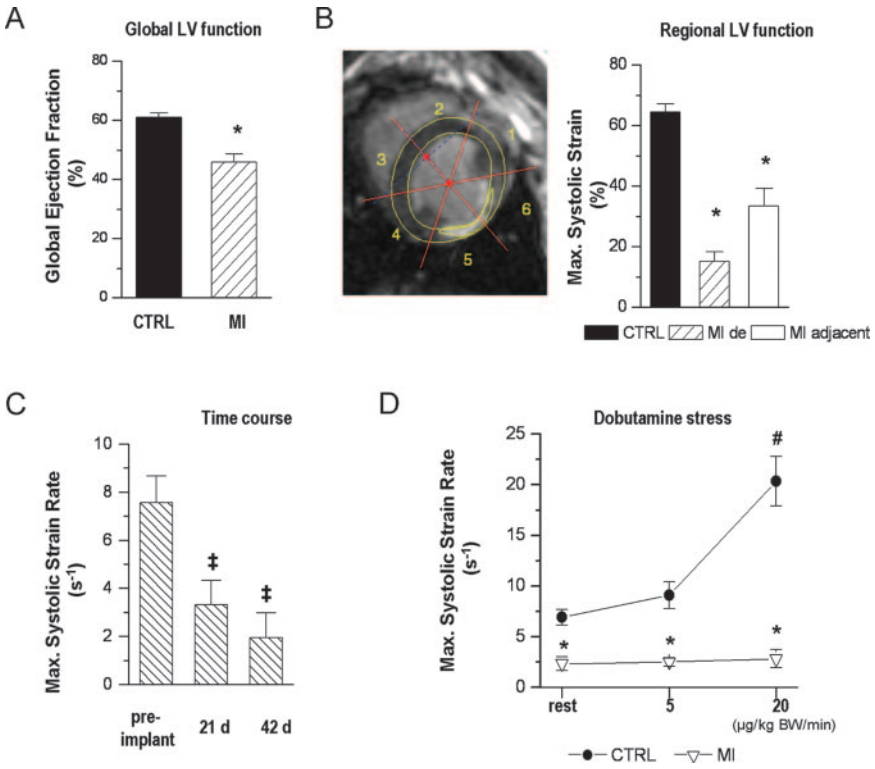

Figure 1. In vivo myocardial function. A, Global LV ejection fraction in MI animals (n=9) compared with CTRL (n=7). B, Example of MRI short axis view with segmentation, contouring of the epi- and endocardial borders and of the delayed enhancement in the inferolateral and anterolateral segments. Regional myocardial function is quantified in the segments with delayed enhancement (MI-de), the adjacent segments within the circumflex artery territory (MI-adjacent), and the analog segments in control animals (CTRL). C, Maximal systolic strain rate in the inferolateral wall during Doppler myocardial velocity imaging in the MI group at 6 weeks after stent implantation, compared with baseline values in the same animals (preimplant). D, Maximal systolic strain rate (myocardial velocity imaging) at rest and in response to dobutamine. ‡$P<0.05$ vs preimplant, *$P<0.05$ vs CTRL, #$P<0.05$ vs rest.

Even in the presence of a normal SR Ca^{2+} content, defective coupling between Ca^{2+} influx and activation of RyR could lead to reduced Ca^{2+} release.[16] Dyssynchronous opening of RyRs and decreased $[Ca^{2+}]_i$ transients were observed in a rabbit model of postinfarct remodeling,[17] and, in this model, a reduction of the L-type Ca^{2+} current (I_{CaL}) was seen; such a reduced I_{CaL} has been reported in other[18,19] but not all models of MI.[20]

Efficient coupling of Ca^{2+} influx through sarcolemmal Ca^{2+} channels (dihydropyridine receptors) and activation of RyRs in the SR is related to the structural organization in couplons, which, in ventricular cardiomyocytes, are found to a large extent along the T-tubules.[21] Experimentally reducing T-tubule density indeed leads to dyssynchronous intracellular Ca^{2+} release and reduced $[Ca^{2+}]_i$ transients.[22–24] A loss of T-tubules could be part of the postinfarction remodeling process. In end-stage human heart failure, histological examination showed dilation of T-tubules[25,26] with an increase[25] or decrease[26] in the density of T-tubules in tissue sections. Studies on intact living human ventricular myocytes have not yet been conclusive as to whether T-tubule density is altered,[24,27,28] but the contribution of alterations in T-tubules to remodeling is supported by observations in animal models of heart failure.[29–31]

In this study, we investigated potential changes in T-tubule density and their impact on intracellular Ca^{2+} release in a pig model of severe chronic coronary stenosis with regional myocardial dysfunction and limited infarction without heart failure.

Materials and Methods

An expanded Materials and Methods section is available in the online data supplement at http://circres.ahajournals.org.

Animal Model

A detailed description is provided in the online data supplement. Briefly, a copper-coated stent was inserted into the proximal circumflex artery of young domestic pigs (20 to 25 kg) to induce intima proliferation and severe nonthrombotic coronary stenosis, quantified during coronary angiography. Global and regional left ventricular (LV) function were evaluated at baseline and at 3 and 6 weeks after stent implantation using color Doppler myocardial velocity imaging at baseline and during dobutamine stress. In a number of animals, MRI was used to assess global and regional LV function[4] and to quantify MI as a fraction of total LV mass. The stent implantation induces a severe but slightly variable stenosis and degree of LV dysfunction. In the present study, we used only animals with documented small transmural infarctions; their functional characteristics are shown under Results.

At the time of euthanasia (47±1 days after stent implantation), pigs with MI (N=13) weighed 51±2 kg; matched healthy pigs were used as controls (CTRL) (N=15; weight, 55±4 kg).

Isolation of Cardiac Myocytes

The procedure for isolating myocytes was as described previously.[32] After enzymatic digestion of the tissue wedge perfused by the stenotic artery, the infarct area and 5 to 10 mm around the infarct core were discarded; midmyocardial cells from the remaining digested tissue were used. Myocytes isolated from the midmyocardial layer of the posterior wall of the weight-matched healthy pigs served as controls.

Subcellular $[Ca^{2+}]_i$ Measurements and T-Tubule Quantification

The setup for confocal imaging was as described previously, and image acquisition and analysis is detailed in the online data supplement. $[Ca^{2+}]_i$ transients were recorded during steady-state stimulation at 1 Hz, with depolarizing steps from −70 to 0 mV for 150 ms along a line through the center parallel to the long axis of the cell as described previously[24,33]; temporal resolution was 1.54 ms per line, and pixel size (x, y) was 0.2 to 0.4 μm. For T-tubule density (di-8-ANEPPS [di-8-butyl-amino-naphthyl-ethylene-pyridinium-

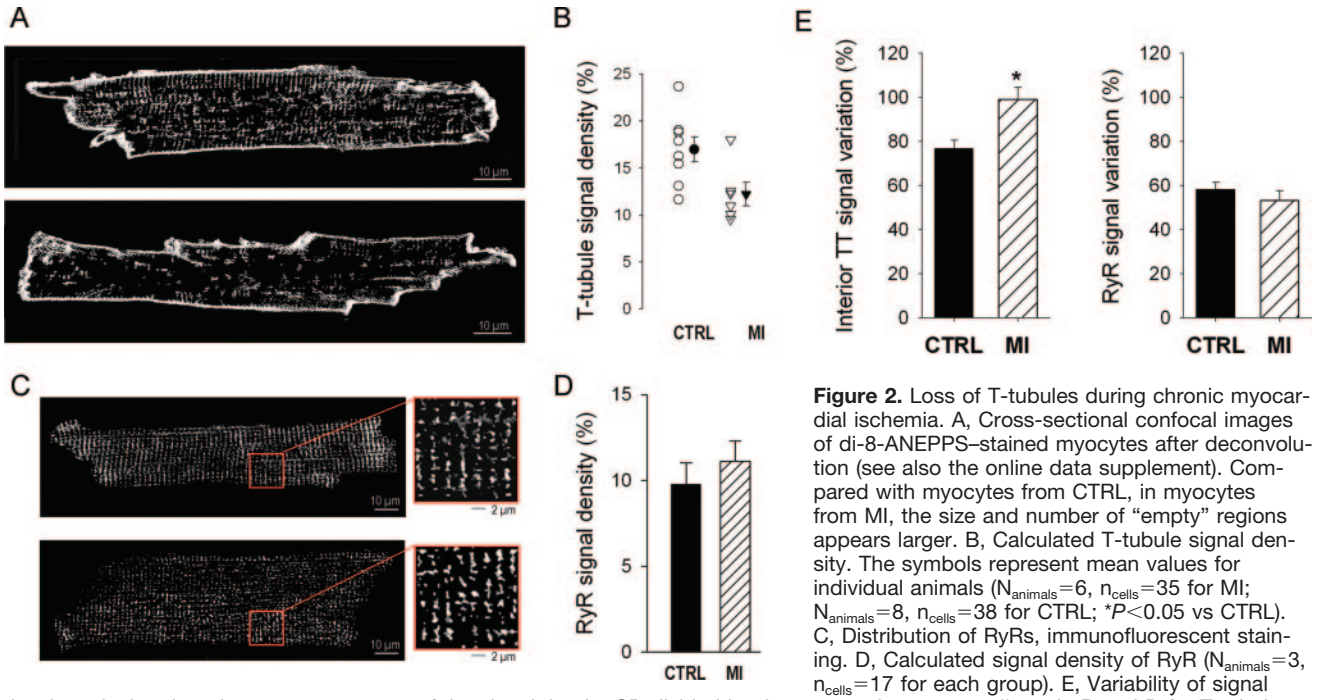

Figure 2. Loss of T-tubules during chronic myocardial ischemia. A, Cross-sectional confocal images of di-8-ANEPPS–stained myocytes after deconvolution (see also the online data supplement). Compared with myocytes from CTRL, in myocytes from MI, the size and number of "empty" regions appears larger. B, Calculated T-tubule signal density. The symbols represent mean values for individual animals ($N_{animals}=6$, $n_{cells}=35$ for MI; $N_{animals}=8$, $n_{cells}=38$ for CTRL; $^*P<0.05$ vs CTRL). C, Distribution of RyRs, immunofluorescent staining. D, Calculated signal density of RyR ($N_{animals}=3$, $n_{cells}=17$ for each group). E, Variability of signal density calculated as the percentage error of the signal, ie, the SD divided by the mean value; same cells as in B and D for T-tubules and RyR, respectively.

propyl-sulfonate] staining) 8 to 10 sequential xy images centered around the equatorial plane of the cell were recorded from each cell, with a spacing of 1 μm in the z-direction and a pixel width of 0.11 to 0.20 μm.

Global $[Ca^{2+}]_i$ and Membrane Current Measurements

The setup for epifluorescence recording, protocols, and solutions are described in the online data supplement.

Immunofluorescence Imaging and Western Blot

The procedures are described in the online data supplement. For protein expression, we used transmural needle biopsies from the ischemic area taken in situ at the time of euthanasia. Control tissue was obtained from the same area in hearts of CTRL pigs.

Image Analysis

Algorithms to analyze the spatial and temporal characteristics of the $[Ca^{2+}]_i$ transients were custom-made (IDL 6.1, Research Systems International, Paris, France); the approaches are detailed in the online data supplement. All temporal data refer to the onset of the whole-line averaged $[Ca^{2+}]_i$ transient. F_{50} was defined as the half-maximum of the normalized overall peak $[Ca^{2+}]_i$-dependent fluorescence and served as a threshold to discriminate local Ca^{2+} release as described previously.[33] To evaluate T-tubules, the images were deconvolved and automatically thresholded; the sarcolemmal surface membrane was excluded from analysis in all images (more details are available in online data supplement). T-tubule density is expressed as the fraction of positive pixels of all pixels within the sarcolemmal boundaries; data are per cell and subsequently pooled per animal.

Statistics

Data are shown as means±SEM and were compared using Student's *t* test or 2-way ANOVA; Fisher's least-significant difference test was performed when significant overall effects were detected. $P<0.05$ was considered significant.

Results

Global and Regional LV Function In Vivo

The degree of circumflex arterial stenosis was 91±3% of the vessel lumen. At 6 weeks, LV ejection fraction at rest, as determined from MRI, was slightly but significantly decreased in MI versus CTRL (Figure 1A); the LV end-diastolic volume was not increased (116±10 mL in MI versus 106±10 mL in CTRL, $P=0.1$). Infarction, as determined from the delayed enhancement images (Figure 1B), comprised 8.8±2.0% of the total LV mass; this corresponds to ≈50% of the area at risk. MRI confirmed the regional dysfunction in the segments with delayed enhancement as well as in the adjacent segments within the area subtended by the stenotic artery (Figure 1B).

Myocardial velocity imaging during follow-up showed the regional dysfunction present at 3 weeks as a severely reduced systolic strain rate (Figure 1C). At 6 weeks, there was no inotropic response to dobutamine (Figure 1D), consistent with the presence of transmural MI.[34]

(Ultra)structural Remodeling of Myocytes

Cardiomyocytes from the MI adjacent area were hypertrophied, as indicated by a significant increase in cell length: 186±6 μm in MI ($N_{animals}=9$, $n_{cells}=254$) versus 147±6 μm in CTRL ($N_{animals}=6$, $n_{cells}=180$, $P<0.05$). Cell width and cell depth tended to be increased as well (29±2 versus 28±1 μm in CTRL, $P=0.2$; 22±1 versus 18±1 μm in CTRL, $P=0.07$). The calculated increase of cell volume assuming a brick-like shape for MI was 51%. This contrasts with the increase of total, ie, external and T-tubular, membrane area measured from the cell capacitance of 30% from 91±5 pF (CTRL: $N_{animals}=9$, $n_{cells}=65$) to 118±8 pF (MI: $N_{animals}=5$, $n_{cells}=43$, $P<0.05$).

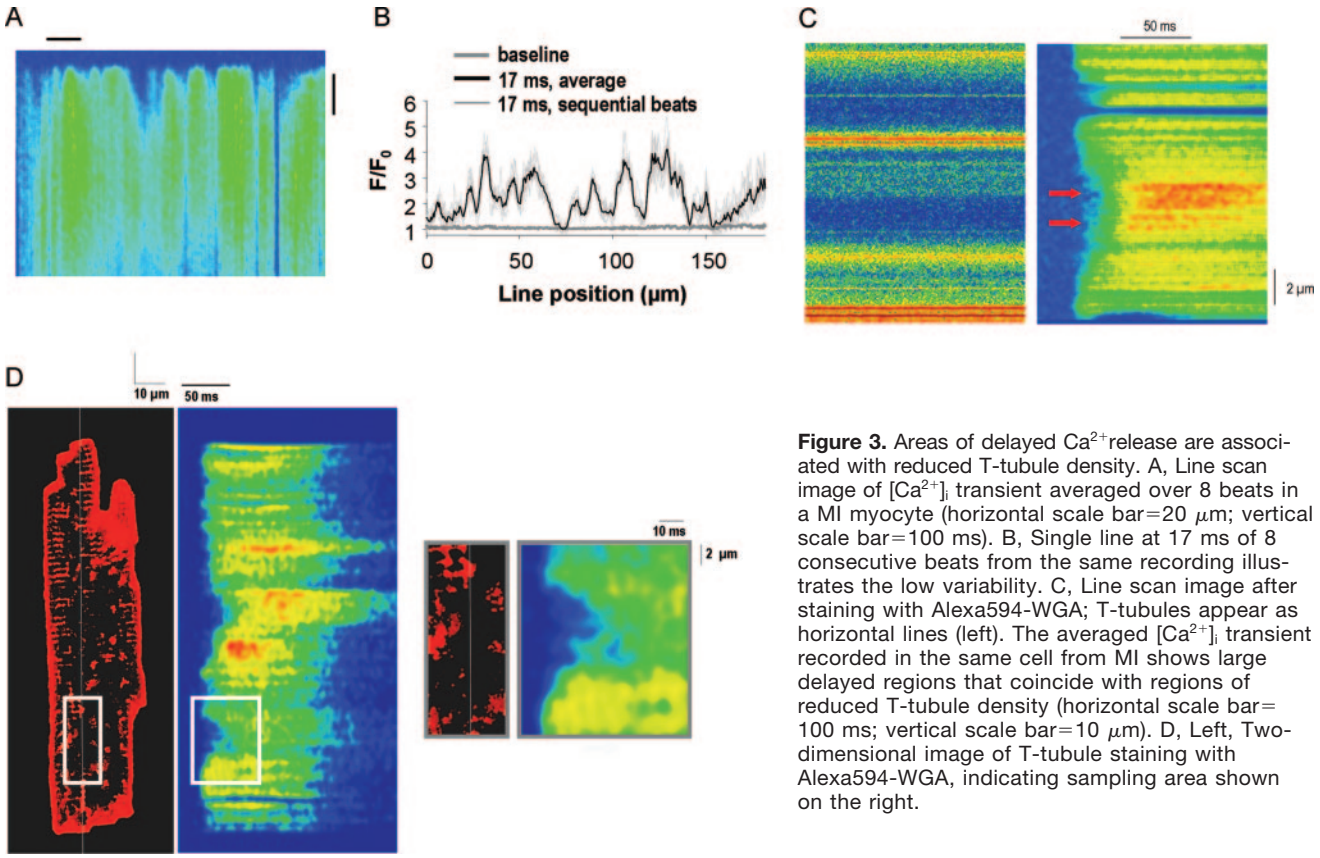

Figure 3. Areas of delayed Ca^{2+}release are associated with reduced T-tubule density. A, Line scan image of $[Ca^{2+}]_i$ transient averaged over 8 beats in a MI myocyte (horizontal scale bar=20 μm; vertical scale bar=100 ms). B, Single line at 17 ms of 8 consecutive beats from the same recording illustrates the low variability. C, Line scan image after staining with Alexa594-WGA; T-tubules appear as horizontal lines (left). The averaged $[Ca^{2+}]_i$ transient recorded in the same cell from MI shows large delayed regions that coincide with regions of reduced T-tubule density (horizontal scale bar= 100 ms; vertical scale bar=10 μm). D, Left, Two-dimensional image of T-tubule staining with Alexa594-WGA, indicating sampling area shown on the right.

T-tubule density expressed as the fraction of positive pixels of all pixels within the sarcolemmal boundaries was significantly reduced in MI (Figure 2). Expressed as a fraction of the external sarcolemmal boundary, the values were also close to significance (0.77 ± 0.05 versus 0.92 ± 0.06 μm^{-1} in CTRL, $P=0.057$). In contrast, the intracellular distribution of RyR appeared homogeneous and similar in CTRL and MI (Figure 2C). This was quantified by measuring RyR signal density, which was similar in cells from CTRL ($N_{animals}=3$, $n_{cells}=17$) and MI ($N_{animals}=5$, $n_{cells}=17$; Figure 2D). We also examined the variability in either RyR or T-tubule signal in individual 5×5 μm boxed areas of a cell (detailed in the online data supplement), as regional loss would result in a higher variability. Here, again, there was a significant difference between MI and CTRL for T-Tubules but not for RyR (Figure 2E).

Reduced Synchrony of Ca^{2+} Release

During confocal line scan imaging of the $[Ca^{2+}]_i$ transient, myocytes from MI had numerous areas with delayed Ca^{2+} release, persistently present during consecutive pulses, as evident in the $[Ca^{2+}]_i$ transient averaged over 10 beats (Figure 3A). The absence of beat-to-beat variability is further illustrated in Figure 3B, showing the line at 17 ms during sequential beats and the small extent of variability in this line. In myocytes in which the sarcolemma was stained with wheat germ agglutinin (WGA)-Alexa594, a first line scan using the 543 nm excitation showed T-tubules as continuous lines of constant intensity (Figure 3C, left); during the subsequent line scan using the 488 nm excitation of fluo-3, the regions of delayed Ca^{2+} release could be related to areas of T-tubule rarefaction (Figure 3C, right). Figure 3D shows another cell with the 2D WGA-Alexa594 image and the area from which the recording was made.

We hypothesized that these regions of delayed Ca^{2+} release lead to a slowed upstroke of the $[Ca^{2+}]_i$ transient in MI. This was quantified by measuring for each consecutive line scan the fraction of the line that had a fluorescence larger than 50% of the maximal ($F>F_{50}$).[33] As shown in Figure 4A, in MI cells, this proceeded more slowly than in CTRL, and, at 20 ms, Ca^{2+} release remained below F_{50} along $36.7\pm5.7\%$ of the line in MI versus only $22.7\pm2.5\%$ of the line in CTRL ($P<0.05$). Likewise, the time to peak of the $[Ca^{2+}]_i$ transient, spatially averaged over the entire line, was longer in MI (122 ± 8 ms, $N_{animals}=8$, $n_{cells}=35$ versus 102 ± 5 ms, $N_{animals}=13$, $n_{cells}=41$ in CTRL, $P<0.05$).

Increased inhomogeneity in Ca^{2+} release in MI cells was attributable to a larger number (Figure 4B), as well as a larger size (Figure 4C), of the regions of delayed Ca^{2+} release.

We further examined the properties of Ca^{2+} release within both early and delayed regions. Time to local peak $[Ca^{2+}]_i$ in regions of early Ca^{2+} release was not different in MI versus CTRL (66 ± 9 versus 74 ± 8 ms, $n_{cells}=17$ and 14), and amplitude was also not different (F/F_0 3.2 ± 0.2 versus 3.4 ± 0.3). In areas of delayed release, the Ca^{2+} release was shown previously to propagate in a wave-like manner because of Ca^{2+}-induced Ca^{2+} release.[24] In the current study, this process was quantified as the rate of filling (decrease in width as a function of time) for regions

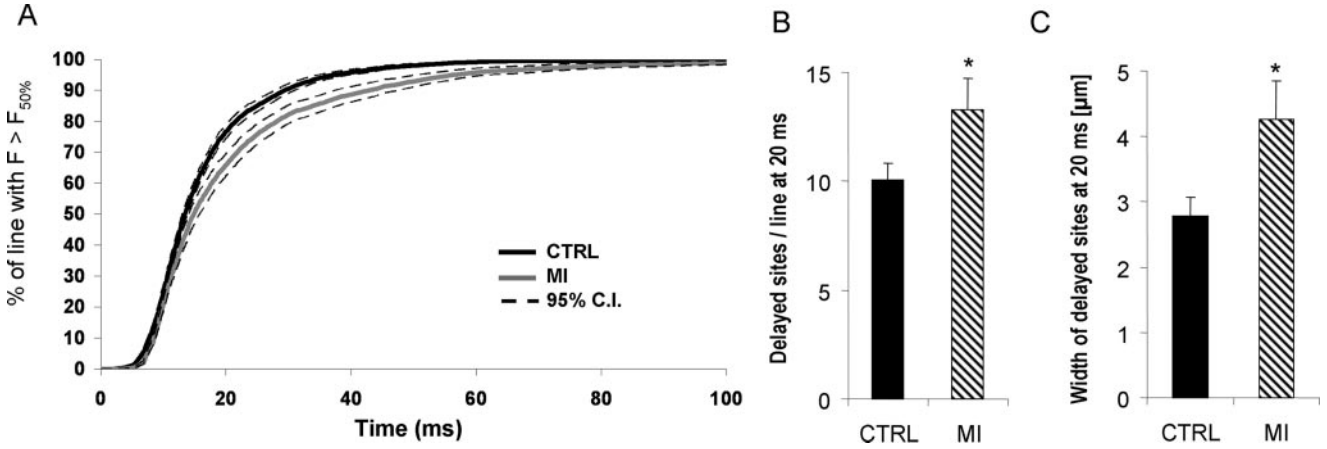

Figure 4. Reduced synchrony leads to slower rise of $[Ca^{2+}]_i$ in myocytes from MI. A, The fraction of the scan line with at least half-maximal Ca^{2+} release is shown as a function of time (dashed lines indicate 95% confidence interval); the curve from MI is less steep. B and C, The width of regions with delayed Ca^{2+} release ($F<F_{50}$) was quantified 20 ms after the onset of the overall $[Ca^{2+}]_i$ transient. Both number (B) and size (C) of delayed regions are larger in MI cells. *$P<0.05$ vs CTRL.

of delayed Ca^{2+} release with a width of >5 μm (n=35 in MI and n=20 in CTRL), as illustrated in Figure 5A. No difference in rate of filling was found between MI and CTRL (Figure 5B).

We also examined whether cAMP-mediated positive inotropic stimulation could synchronize Ca^{2+} release in early and delayed Ca^{2+} release sites. As demonstrated in Figure 6A and 6B, the amplitude of Ca^{2+} release was greatly increased in the presence of forskolin (top); the extent and distribution of delayed Ca^{2+} release sites however appeared unchanged (bottom). Quantitative analysis of local $[Ca^{2+}]_i$ transients (n_{cells}=9) confirmed that the fraction of delayed release areas was unchanged (41±7 versus 33±6% at baseline). Time to peak $[Ca^{2+}]_i$ in regions defined as delayed before the addition of forskolin remained significantly longer than in early regions also in the presence of the drug. The response to forskolin was not different in MI from CTRL (Figure 6C).

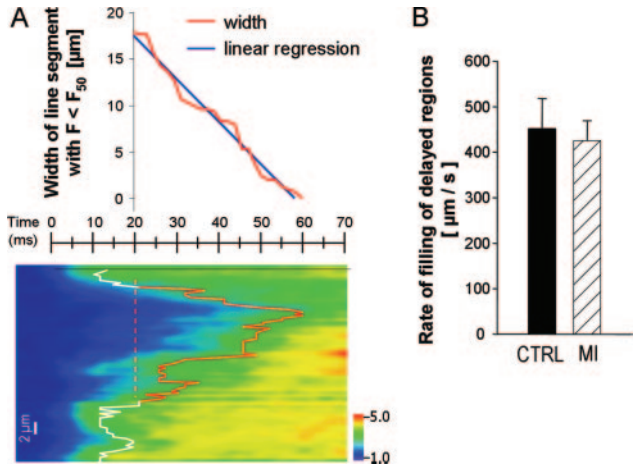

Figure 5. Kinetics of Ca^{2+} release in delayed areas. A, The rate of filling of the delayed regions was quantified by linear regression (in the example: slope, 475 μm/sec; r=0.9887) of the width of the region over time. The red solid line in the line scan image indicates the time points at which F reaches F_{50}. B, The rate of filling of delayed regions was not different between CTRL (n_{cells}=20) and MI (n_{cells}=34).

Reduced Overall Gain of SR Ca^{2+} Release in MI

In a subset of animals (N=4 for MI, N=5 for CTRL), the whole-cell averaged $[Ca^{2+}]_i$ transients were studied in a epifluorescence setup. Peak $[Ca^{2+}]_i$ during steps from −70 to +10 mV, as used in the confocal analysis, was lower in MI (n_{cells}=12) versus CTRL (n=15, $P<0.05$; Figure 7A), and the time to peak $[Ca^{2+}]_i$ was prolonged (Figure 7B). The density of the L-type Ca^{2+} current was not significantly different (Figure 7C).

Because the $[Ca^{2+}]_i$ transients were of lower amplitude despite unchanged Ca^{2+} current, a reduction of SR content was expected, and this was tested using caffeine to release all SR Ca^{2+}; Figure 8A shows the averaged signals of $[Ca^{2+}]_i$ and inward NCX current for all MI (n_{cells}=12) and CTRL myocytes (n_{cells}=15). The integral of the inward NCX current ($\int I_{NCX}$) during caffeine application (Figure 8B) was unexpectedly increased in MI versus CTRL, suggesting an increased Ca^{2+} content of the SR. In contrast, the caffeine-induced peak $[Ca^{2+}]_i$ was reduced in MI (Figure 8C). These latter observations may rather reflect altered kinetics of Ca^{2+} release from the SR in response to caffeine in MI cells, as time to peak (Figure 8D) of the caffeine-induced $[Ca^{2+}]_i$ transient was significantly increased in MI versus CTRL. The rate of decay was also significantly increased (Figure 8E), reflecting a reduced rate of Ca^{2+} removal by the NCX. Yet global protein expression of the NCX was unaltered (Figure 8F).

We analyzed the properties of spontaneous release events or sparks, observed in a 15-second period following stimulation at 1 Hz (for MI: $N_{animals}$=7, n_{cells}=36, 2472 sparks; for CTRL: $N_{animals}$=12, n_{cells}=44, 2280 sparks). In MI animals, 100% of cells had spontaneous release events versus 74% in CTRL ($P<0.05$), but analysis of mean frequency was not statistically different (1.69±0.35 versus 1.27±0.23 sparks/sec per 100 μm in CTRL). Amplitude and duration were also not statistically different (F/F_0, 1.76±0.05 versus 1.70±0.06

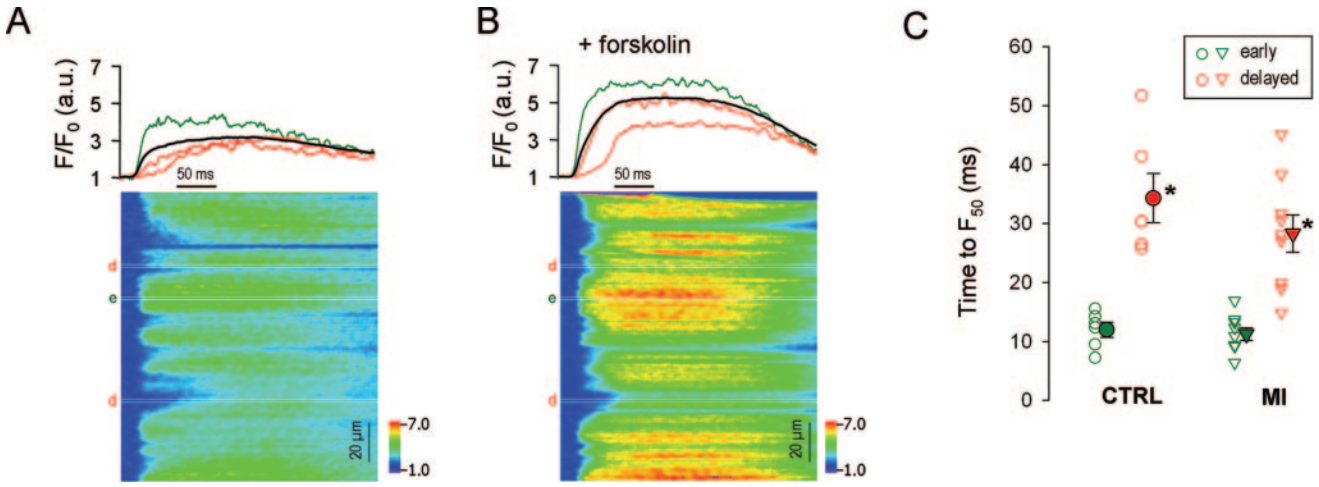

Figure 6. Persistent delayed Ca^{2+} release in the presence of forskolin. A and B, Line scan images of a beat-to-beat-averaged $[Ca^{2+}]_i$ transient in a MI cardiomyocyte in control conditions (A) and in the presence of forskolin (10 μmol/L) (B). The overall $[Ca^{2+}]_i$ transient is represented by the black curve; early local $[Ca^{2+}]_i$ transients are marked as "e" by the green curve, and delayed transients are marked as "d" by the green curves. a.u. indicates arbitrary units. C, Time to peak $[Ca^{2+}]_i$ of local $[Ca^{2+}]_i$ transients in the presence of forskolin; open symbols represent individual cells. *$P<0.05$ vs CTRL.

in CTRL; full duration at half-magnitude, 39±2 versus 36±2 ms in CTRL).

Discussion

In Vivo Function and Remodeling With Chronic Coronary Stenosis

The most commonly used models for cellular remodeling after MI rely on smaller animals with ligation of a coronary artery, usually the left anterior descending. In these animals, MI typically is large, leading to heart failure (eg, in the rat[35] and rabbit[36]). In the current animal model, we have a limited infarction within a larger area of chronic underperfusion; at 6 weeks, the impact on global function is present but limited. Therefore, this model allows us to study the changes with chronic ischemia in the area adjacent to the infarct, before the onset of heart failure. One can then question whether this is essentially different from the condition we have studied previously, namely hibernation, where there is no or only very limited subendocardial necrosis. We think, at present, these data should not be mixed. The regional contractile function in the hibernating myocardium is less affected because the loss of contractile cells is small. This implies that mechanical loading on the remaining myocytes is less than in the presence of MI, which could lead to different stimuli for remodeling.

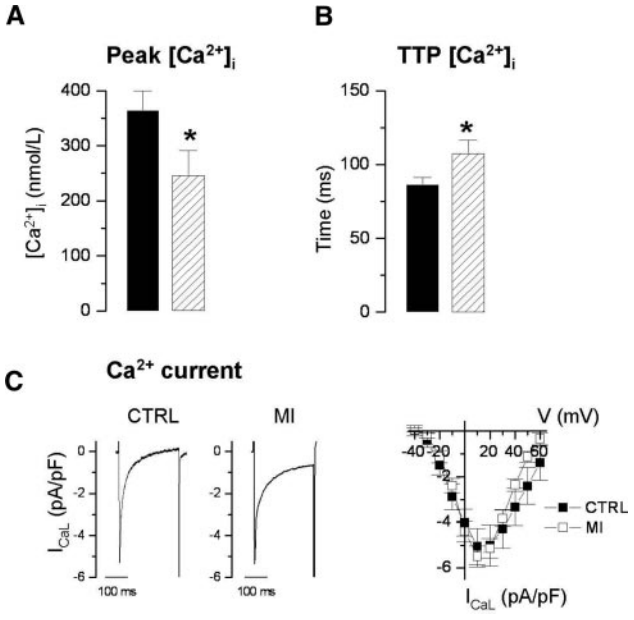

Figure 7. Whole-cell-averaged $[Ca^{2+}]_i$ transients and Ca^{2+} current. A, Peak $[Ca^{2+}]_i$ following a 225-ms step from −70 to +10 mV (1 Hz) was decreased in MI ($n_{cells}=12$) vs CTRL myocytes ($n_{cells}=15$). B, Time to peak $[Ca^{2+}]_i$ was increased. C, L-type Ca^{2+} current density (I_{CaL}), measured as the peak inward nifedipine-sensitive current component, was unchanged in MI ($n_{cells}=10$) vs CTRL ($n_{cells}=11$).

We currently have a limited number of data to sustain that there is a difference in cellular remodeling in cardiomyocytes from hibernating myocardium as compared with cells from the area adjacent to the infarct. At the whole-cell level, the overall $[Ca^{2+}]_i$ transients are more affected in the present dataset than in our earlier group of hibernation,[32] although the Ca^{2+} current in the present study was less affected. There are also a number of similarities because SR Ca^{2+} content was similarly preserved. We currently have no data on subcellular synchrony of release in hibernating myocardium, but preliminary data also have shown a reduction in T-tubule density. Cellular hypertrophy is present in both groups.

Remodeling of T-Tubules

Ventricular myocytes develop T-tubules after birth,[37] whereas atrial myocytes or Purkinje cells do not.[38–40] The density of the T-tubule system is variable between species, and T-tubules disappear during culture of adult cardiac myocytes.[23,24,33] These observations indicate that the T-tubule system is under active regulation and that it could change with disease. Yet the observations of remodeling with disease are limited.[29–31] The present data document a lower density of

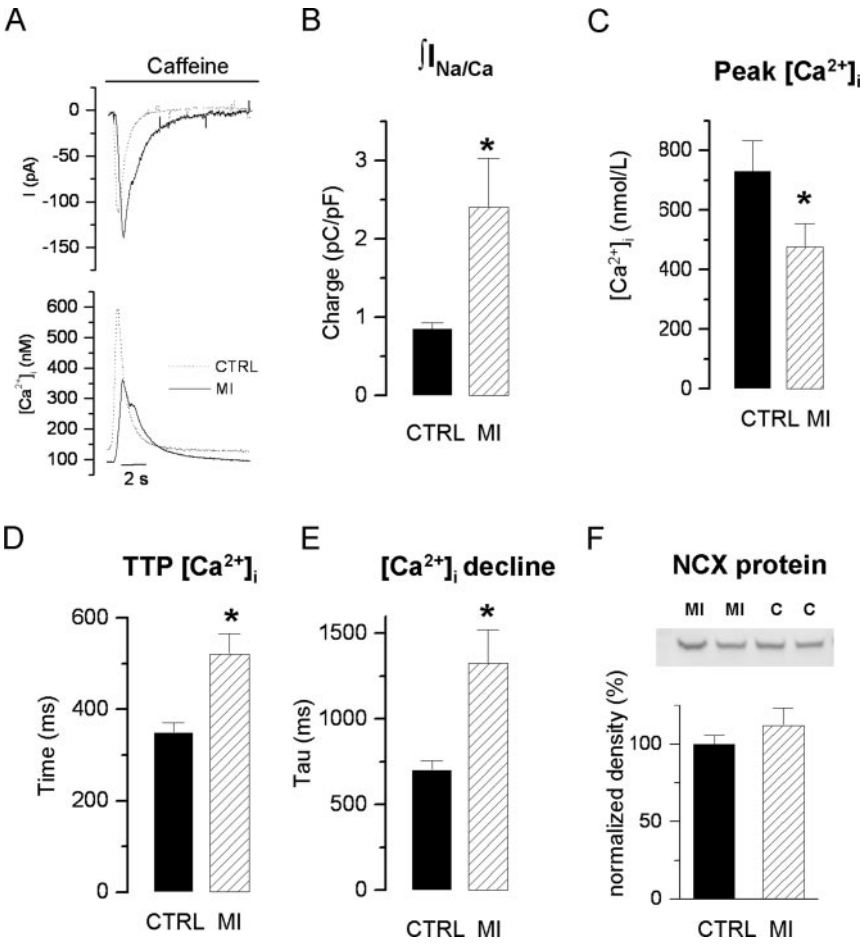

Figure 8. SR Ca^{2+} content. A, Averaged traces of $[Ca^{2+}]_i$ transients and NCX currents during a 10-second caffeine application following a conditioning train of 10 depolarizing steps from −70 to +10 mV at 1 Hz; the same cells as in Figure 7A and 7B (12 MI cells and 15 CTRL cells). B, SR Ca^{2+} content, as estimated from the integral of the NCX current (I_{NCX}), was increased in MI. C, The peak caffeine-induced $[Ca^{2+}]_i$ was reduced in MI. D, Time to peak $[Ca^{2+}]_i$ of the caffeine-induced Ca^{2+} release. E, Tau values for exponential fit of the decline of $[Ca^{2+}]_i$. F, Protein levels of NCX measured in immunoblot; averaged data for 5 vs 5 samples. All data are normalized to the average signal intensity of the CTRL samples. *$P<0.05$ vs CTRL.

T-tubules during ischemic remodeling before the development of heart failure.

This does not necessarily represent a net loss. Indeed, the myocytes were clearly hypertrophied, and the lower density of T-tubules could represent a differential growth and organization of this organelle in relation to the addition of sarcomeres. A striking finding was also that the distribution of RyR was unchanged. The data thus support the idea that T-tubules have a degree of plasticity and can undergo remodeling independent of the organization of the SR.

Song et al[31] observed reorganization of T-tubules in spontaneously hypertensive rats, with a decrease in the transverse tubules in favor of an increase in the longitudinal tubules; the authors did not report a decrease in overall density. Similar observations were made in the mouse.[30] This could be related to the different stimulus for remodeling but also to differences in small versus large animals. The rat, like the mouse, has a very dense network, possibly related to high heart rates, whereas pigs have a lower density, more like humans.[24,33] In the latter system, reorganization may be more likely to result in true loss of T-tubules in certain areas.

Reduced Synchrony of Ca^{2+} Release

Litwin et al were the first to describe dyssynchronous Ca^{2+} release in myocytes from failing rabbit hearts after MI.[17] In their study, Ca^{2+} release had a beat-to-beat regional variation, and release events were observed to occur late during depolarization. This dyssynchrony was linked to a reduced I_{CaL} and the presence of functional couplons with decreased triggering; it could be rescued at least partially by protein kinase A–dependent phosphorylation and increased activity of I_{CaL}. In a model of right ventricular failure, a reduction in I_{Ca} associated with changes in early repolarization also resulted in a regional beat-by-beat variation in intracellular Ca^{2+} release.[41] The current study points to a different mechanism underlying reduced synchrony of Ca^{2+} release. First, we studied Ca^{2+} release during square voltage-clamp pulses, eliminating the influence of potential changes in early repolarization. Second, we focused on regions where Ca^{2+} release was persistently delayed in sequential $[Ca^{2+}]_i$ transients, independent of beat-to-beat variability. We could not "rescue" the delayed release by increasing cAMP. In contrast, we could link the delayed release sites to areas of low T-tubule density. These data are consistent with a structural alteration. Recent computational analysis supports the importance of small changes in the structures relating dihydropyridine receptor and RyR.[42]

We also considered the possibility of a reduction in couplon size, which would result in a longer latency and reduced probability of release at spark sites.[43] This additional analysis is presented in the online data supplement. The data suggest that, in addition to the larger number of delayed release sites, increased dyssynchrony at presumed spark sites is present. This could result from a smaller couplon size.

Additional experiments are needed to evaluate the contribution of these changes to the overall reduced synchrony.

Coupling Efficiency Between Dihydropyridine Receptor and RyR and the Role of T-Tubules

The consequences of reduced synchrony are a global slowing of the rate of rise of $[Ca^{2+}]_i$, as also observed in the spatially averaged whole-cell $[Ca^{2+}]_i$ transients. In such recordings, the longer time to peak, in particular together with the reduced amplitude of the $[Ca^{2+}]_i$ transient, indicates that, overall, the SR Ca^{2+} release is reduced, despite preserved global Ca^{2+} influx and SR Ca^{2+} content. This can be interpreted as a reduced efficiency of coupling, as was initially proposed in the rat with hypertension-induced heart failure.[44]

Reduced coupling efficiency in MI may be the result of a smaller fraction of existing RyRs that are activated, because of a lack of T-tubules and possibly because of a reduction in couplon size. The distribution of RyRs was preserved, and the propagation of Ca^{2+} release within the delayed areas was the same for MI and CTRL, as were the properties of sparks, suggesting that the intrinsic properties of the RyR were not altered.

The presence of RyRs that are not coupled to the dihydropyridine receptor has analogies with experimentally reducing the probability of activating the RyR, eg, with low doses of caffeine or by reducing the activation of Ca^{2+} channels.[45,46] Under those conditions, the SR can (locally) become overloaded, and this can give rise to even more pronounced heterogeneity in release under the form of alternans. This was currently not observed, but the larger SR content could be the result of reduced RyR activation.

The slower decay of the caffeine transient points toward a reduced efficiency in Ca^{2+} removal. This was also noticed in studies with acute detubulation[22] and during cell culture.[24] The reduced rate of rise of $[Ca^{2+}]_i$ with caffeine application in MI myocytes might be related to reduced T-tubule density, because we likewise noted a significant increase in time to peak of 50%, with a 60% reduction of T-tubule density in cultured myocytes (data from Louch et al[24]). Alternatively, this may indicate additional changes in RyR properties, with a reduced response to caffeine.

Conclusions

In myocytes from the area adjacent to MI, decreased T-tubule density is associated with reduced global coupling efficiency, reduced synchrony of Ca^{2+} release, and slowed and reduced cellular $[Ca^{2+}]_i$ transients. This occurs in the absence of changes in distribution of the RyR and indicates that plasticity of T-tubules is an independent factor in the remodeling process.

Acknowledgments

We thank Patricia Holemans and Pascal Hamaekers for technical assistance and Niall Macquaide (Glasgow University, UK) for the MacSpark analysis program.

Sources of Funding

This study was supported by grants to K.R.S. from the Fund for Scientific Research–Flanders (G.0384.07), the European Union (LSHM-CT-2005-018833, EUGeneHeart), and Belgian Science Program IAP6/31.

Disclosures

None.

References

1. Heidenreich PA, McClellan M. Trends in treatment and outcomes for acute myocardial infarction: 1975–1995. *Am J Med*. 2001;110:165–174.
2. Pfeffer MA. Left ventricular remodeling after acute myocardial infarction. *Annu Rev Med*. 1995;46:455–466.
3. McMurray J, Pfeffer MA. New therapeutic options in congestive heart failure. Part I. *Circulation*. 2003;105:2099–2106.
4. Rademakers F, Van de WF, Mortelmans L, Marchal G, Bogaert J. Evolution of regional performance after an acute anterior myocardial infarction in humans using magnetic resonance tagging. *J Physiol*. 2003; 546:777–787.
5. Beuckelmann DJ, Erdmann E. Ca(2+)-currents and intracellular [Ca2+]i-transients in single ventricular myocytes isolated from terminally failing human myocardium. *Basic Res Cardiol*. 1992;87(suppl 1):235–243.
6. Sipido KR, Stankovicova T, Flameng W, Vanhaecke J, Verdonck F. Frequency dependence of Ca^{2+} release from the sarcoplasmic reticulum in human ventricular myocytes from end-stage heart failure. *Cardiovasc Res*. 1998;37:478–488.
7. Piacentino V, III, Weber CR, Chen X, Weisser-Thomas J, Margulies KB, Bers DM, Houser SR. Cellular basis of abnormal calcium transients of failing human ventricular myocytes. *Circ Res*. 2003;92: 651–658.
8. Kim YK, Kim SJ, Kramer CM, Yatani A, Takagi G, Mankad S, Szigeti GP, Singh D, Bishop SP, Shannon RP, Vatner DE, Vatner SF. Altered excitation-contraction coupling in myocytes from remodeled myocardium after chronic myocardial infarction. *J Mol Cell Cardiol*. 2002; 34:63–73.
9. Licata A, Aggarwal R, Robinson RB, Boyden PA. Frequency dependent effects on Ca_i transients and cell shortening in myocytes that survive in the infarcted heart. *Cardiovasc Res*. 1997;33:341–350.
10. Litwin SE, Bridge JHB. Enhanced Na^+-Ca^{2+} exchange in the infarcted heart. Implications for excitation-contraction coupling. *Circ Res*. 1997; 81:1083–1093.
11. Neary P, Duncan AM, Cobbe SM, Smith GL. Assessment of sarcoplasmic reticulum Ca(2+) flux pathways in cardiomyocytes from rabbits with infarct-induced left-ventricular dysfunction. *Pflugers Arch*. 2002; 444:360–371.
12. Zhang XQ, Ng YC, Moore RL, Musch TI, Cheung JY. In situ SR function in postinfarction myocytes. *J Appl Physiol*. 1999;87:2143–2150.
13. Yue P, Long CS, Austin R, Chang KC, Simpson PC, Massie BM. Post-infarction heart failure in the rat is associated with distinct alterations in cardiac myocyte molecular phenotype. *J Mol Cell Cardiol*. 1998;30:1615–1630.
14. Gomez AM, Schwaller B, Porzig H, Vassort G, Niggli E, Egger M. Increased exchange current but normal Ca2+ transport via Na+-Ca2+ exchange during cardiac hypertrophy after myocardial infarction. *Circ Res*. 2002;91:323–330.
15. Currie S, Quinn FR, Sayeed RA, Duncan AM, Kettlewell S, Smith GL. Selective down-regulation of sub-endocardial ryanodine receptor expression in a rabbit model of left ventricular dysfunction. *J Mol Cell Cardiol*. 2005;39:309–317.
16. Gomez AM, Guatimosim S, Dilly KW, Vassort G, Lederer WJ. Heart failure after myocardial infarction: altered excitation-contraction coupling. *Circulation*. 2001;104:688–693.
17. Litwin SE, Zhang D, Bridge JHB. Dyssynchronous Ca^{2+} sparks in myocytes from infarcted hearts. *Circ Res*. 2000;87:1040–1047.
18. Dun W, Baba S, Yagi T, Boyden PA. Dynamic remodeling of K+ and Ca2+ currents in cells that survived in the epicardial border zone of canine healed infarcted heart. *Am J Physiol Heart Circ Physiol*. 2004; 287:H1046–H1054.
19. Santos PE, Barcellos LC, Mill JG, Masuda MO. Ventricular action potential and L-type calcium channel in infarct-induced hypertrophy in rats. *J Cardiovasc Electrophysiol*. 1995;6:1004–1014.
20. Qin D, Zhang ZH, Caref EB, Boutjdir M, Jain P, El-Sherif N. Cellular and ionic basis of arrhythmias in postinfarction remodeled ventricular myocardium. *Circ Res*. 1996;79:461–473.

21. Franzini-Armstrong C, Protasi F, Ramesh V. Shape, size, and distribution of Ca(2+) release units and couplons in skeletal and cardiac muscles. *Biophys J*. 1999;77:1528–1539.
22. Brette F, Orchard C. T-tubule function in mammalian cardiac myocytes. *Circ Res*. 2003;92:1182–1192.
23. Lipp P, Huser J, Pott L, Niggli E. Spatially non-uniform Ca2+ signals induced by the reduction of transverse tubules in citrate-loaded guinea-pig ventricular myocytes in culture. *J Physiol (Lond)*. 1996;497: 589–597.
24. Louch WE, Bito V, Heinzel FR, Macianskiene R, Vanhaecke J, Flameng W, Mubagwa K, Sipido KR. Reduced synchrony of Ca^{2+} release with loss of T-tubules - a comparison to human failing cardiac myocytes. *Cardiovasc Res*. 2004;62:63–73.
25. Kaprielian RR, Stevenson S, Rothery SM, Cullen MJ, Severs NJ. Distinct patterns of dystrophin organization in myocyte sarcolemma and transverse tubules of normal and diseased human myocardium. *Circulation*. 2000;101:2586–2594.
26. Kostin S, Scholz D, Shimada T, Maeno Y, Mollnau H, Hein S, Schaper J. The internal and external protein scaffold of the T-tubular system in cardiomyocytes. *Cell Tissue Res*. 1998;294:449–460.
27. Ohler A, Houser SR, Tomaselli GF, O'Rourke B. Transverse tubules are unchanged in myocytes from failing human hearts. *Biophys J*. 2001; 80:590a.
28. Wong C, Soeller C, Burton L, and Cannell MB. Changes in transverse-tubular system architecture in myocytes from diseased human ventricles. *Biophys J*. 2001;80:588a.
29. He J, Conklin MW, Foell JD, Wolff MR, Haworth RA, Coronado R, Kamp TJ. Reduction in density of transverse tubules and L-type Ca(2+) channels in canine tachycardia-induced heart failure. *Cardiovasc Res*. 2001;49:298–307.
30. Louch WE, Mork HK, Sexton J, Stromme TA, Laake P, Sjaastad I, Sejersted OM. T-tubule disorganization and reduced synchrony of Ca2+ release in murine cardiomyocytes following myocardial infarction. *J Physiol*. 2006;574:519–533.
31. Song LS, Sobie EA, McCulle S, Lederer WJ, Balke CW, Cheng H. Orphaned ryanodine receptors in the failing heart. *Proc Natl Acad Sci U S A*. 2006;103:4305–4310.
32. Bito V, Heinzel FR, Weidemann F, Dommke C, van der Velden J, Verbeken E, Claus P, Bijnens B, De Scheerder I, Stienen GJ, Sutherland GR, Sipido KR. Cellular mechanisms of contractile dysfunction in hibernating myocardium. *Circ Res*. 2004;94:794–801.
33. Heinzel FR, Bito V, Volders PG, Antoons G, Mubagwa K, Sipido KR. Spatial and temporal inhomogeneities during Ca2+ release from the sarcoplasmic reticulum in pig ventricular myocytes. *Circ Res*. 2002;91: 1023–1030.
34. Weidemann F, Dommke C, Bijnens B, Claus P, D'hooge J, Mertens P, Verbeken E, Maes A, Van de Werf F, De Scheerder I, Sutherland GR. Defining the transmurality of a chronic myocardial infarction by ultrasonic strain-rate imaging. Implications for identifying intramural viability: an experimental study. *Circulation*. 2003;107:883–888.
35. Sjaastad I, Bokenes J, Swift F, Wasserstrom JA, Sejersted OM. Normal contractions triggered by I(Ca,L) in ventricular myocytes from rats with postinfarction CHF. *Am J Physiol Heart Circ Physiol*. 2002;283: H1225–H1236.
36. McIntosh MA, Cobbe SM, Smith GL. Heterogeneous changes in action potential and intracellular Ca2+ in left ventricular myocyte sub-types from rabbits with heart failure. *Cardiovasc Res*. 2000;45:397–409.
37. Haddock PS, Coetzee WA, Cho E, Porter L, Katoh H, Bers DM, Jafri MS, Artman M. Subcellular [Ca2+]i gradients during excitation-contraction coupling in newborn rabbit ventricular myocytes. *Circ Res*. 1999;85: 415–427.
38. Huser J, Lipsius SL, Blatter LA. Calcium gradients during excitation-contraction coupling in cat atrial myocytes. *J Physiol (Lond)*. 1996;494: 641–651.
39. Cordeiro JM, Spitzer KW, Giles WR, Ershler PE, Cannell MB, Bridge JH. Location of the initiation site of calcium transients and sparks in rabbit heart Purkinje cells. *J Physiol (Lond)*. 2001;531:301–314.
40. Stankovicova T, Bito V, Heinzel F, Mubagwa K, Sipido KR. Isolation and morphology of single Purkinje cells from the porcine heart. *Gen Physiol Biophys*. 2003;22:329–340.
41. Harris DM, Mills GD, Chen X, Kubo H, Berretta RM, Votaw VS, Santana LF, Houser SR. Alterations in early action potential repolarization causes localized failure of sarcoplasmic reticulum Ca2+ release. *Circ Res*. 2005;96:543–550.
42. Cannell MB, Crossman DJ, Soeller C. Effect of changes in action potential spike configuration, junctional sarcoplasmic reticulum micro-architecture and altered t-tubule structure in human heart failure. *J Muscle Res Cell Motil*. 2006;27:297–306.
43. Inoue M, Bridge JH. Variability in couplon size in rabbit ventricular myocytes. *Biophys J*. 2005;89:3102–3110.
44. Gomez AM, Valdivia HH, Cheng H, Lederer MR, Santana LF, Cannell MB, McCune SA, Altschuld RA, Lederer WJ. Defective excitation-contraction coupling in experimental cardiac hypertrophy and heart failure. *Science*. 1997;276:800–806.
45. Diaz ME, Eisner DA, O'Neill SC. Depressed ryanodine receptor activity increases variability and duration of the systolic Ca2+ transient in rat ventricular myocytes. *Circ Res*. 2002;91:585–593.
46. Diaz ME, O'Neill SC, Eisner DA. Sarcoplasmic reticulum calcium content fluctuation is the key to cardiac alternans. *Circ Res*. 2004;94:650–656.

Heinzel et al. Remodeling of T-Tubules after myocardial infarction

Online Supplement

Materials and Methods

Animal Model

Animals were housed and treated according to the Guide for the Care and Use of Laboratory Animals (National Institute of Health, U.S.A.) and experimental protocols were approved by the in-house ethical committee. All interventions were performed under full anesthesia (premedication with tiletamine and zolazepam, 4mg/kg IM and xylazine 0.25mg/kg IM, maintenance anesthesia with propofol IV, 7 mg/kg/hour; additional analgesia with buprenorphine HCl 0.1 mg/kg); pigs were intubated and ventilated with a 1:1 oxygen/air mixture. A copper-coated stent was inserted into the proximal circumflex artery (LCX) of young domestic pigs (20-25 kg) to induce intima proliferation and non-thrombotic coronary stenosis. The day before stent implantation the pigs received 600 mg acetylsalicylic acid and 300 mg clopidogrel as loading dose; the following days they received 300 mg acetylsalicylic acid and 75 mg clopidogrel daily until sacrifice. The degree of stenosis was evaluated as the minimal luminal stent diameter by quantitative coronary angiography.

Echocardiography was performed before and at 3 and 6 weeks after stent implantation (Aplio, Toshiba Medical Systems, Otawara, Japan). Regional contractile function of the basal inferolateral wall of the left ventricle (LV) was quantified by strain rate analysis using color Doppler myocardial velocity imaging, at baseline and during dobutamine stress (5-20 µg/kg/min)[1]. Images were acquired in a long axis parasternal view. Peak systolic radial strain rate and end-systolic radial strain were extracted from

the echocardiographic datasets using custom made software (SPEQLE, Catholic University Leuven, Belgium).

In a number of animals magnetic resonance imaging (MRI) was used to assess global and regional LV function [2] and the extent of myocardial necrosis at 6 weeks. All MRI studies were performed on a 1.5T Siemens Sonata Vision (Siemens Erlangen, Germany). Cine MRI data, using breath-hold balanced steady-state free-precession technique, were obtained in a stack of short-axis views covering the LV, and in the horizontal and vertical long-axis views. Data sets were acquired at rest and during low-dose (5 µg/kg/min) and high-dose (20 µg/kg/min) dobutamine infusion. Epi- and endocardial borders were contoured at end-diastole and end-systole on the short-axis slices using custom-made software (CardioViewer, Catholic University Leuven, Belgium). End-diastolic and end-systolic cavity volume and LV mass were calculated. LV ejection fraction was reported for global ventricular function. Regional function was assessed as the regional systolic radial strain, i.e. wall thickening, and presented in the 17 segments model of the LV [3]. Contrast-enhanced inversion-recovery MRI with delayed imaging was obtained 10-15 min after injection of 0.1 mmol/kg of gadolinium diethylenetriamine-pentaacid (Gd-DTPA). Myocardial infarction was quantified as the fraction of total LV mass showing delayed enhancement [4]. We quantified systolic radial strain in the segments with delayed enhancement (MI-de), the adjacent segments within the CX territory (MI-adjacent), the remote area and the analog segments in control animals (CTRL).

The intima proliferation induced by the copper-coated stent is severe but slightly variable. In thefirst series the stenosis was larger than 90% of the vessel lumen in most animals (7/10). Within this group with high-grade stenosis, 2 animals had a modest decrease of regional strain at baseline with a biphasic response during

incremental dobutamine stress; MRI showed minimal extent of necrosis, less than 2 % of total LV mass in the subendocardial layers. These animals were considered to have hibernating myocardium and functional evaluation using Doppler MVI was consistent with our earlier data [5]; they were not included in the present study. The remaining 5 animals had transmural infarctions and were included in the present study; their functional MRI characteristics are described in the Results section. Another 4 animals with similar functional properties consistent with transmural infarction but without MRI study were also included. In a second series another 4 animals with documented MI during the MRI were included.

At the time of sacrifice (47±1 days after stent implantation) pigs with myocardial infarction (MI, N=13) weighed 51±2 kg; matched healthy pigs were used as controls (CTRL, N=15, weight 55±4 kg)..

Isolation of Cardiac Myocytes

Pigs were anesthetized, intubated and ventilated as described above and an additional bolus of pentobarbital (100 mg/kg IV) was administered; after opening the thorax the heart was quickly excised and placed in ice-cold Tyrode solution. The circumflex coronary artery was cannulated just distal to the stenosis and the myocardium supplied by the stenosed artery was perfused with Ca-free Tyrode and collagenase as previously described [5]. After enzymatic digestion of the tissue wedge, the infarct area and 5-10 mm around the infarct core were discarded; midmyocardial cells from the remaining digested tissue were used. Myocytes isolated from the midmyocardial layer of the posterior wall of the weight-matched healthy pigs served as controls.

Confocal $[Ca^{2+}]_i$ imaging

Cardiac myocytes were placed in a perfusion chamber on the stage of an inverted microscope equipped with a confocal line laser scanning head (Axiovert 100M and

LSM 510, Zeiss, Jena, Germany) and superfused with Tyrode's solution at 37°C. The sample was examined in regular transmitted light, and rod-shaped quiescent cardiomyocytes with clear sarcomeric striations were randomly selected for confocal scanning. Cells were studied in the ruptured whole cell patch clamp mode; the internal solution in the pipette contained the Ca^{2+} indicator fluo-3. $[Ca^{2+}]_i$ transients were recorded during steady state stimulation at 1 Hz with depolarizing steps from -70 to 0 mV for 150 ms along a line through the center parallel to the long axis of the cell as described earlier [6;7]; temporal resolution was 1.54 ms/line and pixel size (x,y) 0.2-0.4 µm. A subset of cardiomyocytes was incubated with Alexa594 wheat-germ agglutinin (excitation at 543 nm, emission > 590 nm) to stain the sarcolemmal membrane before loading the cell with fluo-3 via the patch pipette. This approach allowed visualization of T-tubular structures and $[Ca^{2+}]_i$ transients in the same cell.

To characterize spontaneous release events or sparks, cells were stimulated at 1 Hz with 225 ms square voltage clamp pulses from -70 to +10 mV until steady state. Sparks were recorded after stopping the stimulation, for a period af 15 s. For spark analysis we used an automated detection and measurement algorithm developed by Loughrey et al. [8], based on the work by Cheng et al.[9].

Quantification of the T-tubule network

T-tubule staining

Cardiomyocytes were incubated with the sarcolemmal membrane dye di-8-ANEPPS (2 µmol/L, incubation for 10 min, followed by 10 min wash) and transferred to the stage of the inverted microscope. The cell sample was examined and cells were selected as described for the patch-clamping experiments. After establishing the dimensions of the cell in Z-direction, 10 XY images were recorded, starting 5 µm below the central XY plane of the cell with a Z-axis spacing of 1 µm towards the top

cell surface (pixel width of 0.11 to 0.20 µm in XY direction). In a subset of cells (11 cardiomyocytes in CTRL and 11 cardiomyocytes in MI), XY images at the top or bottom of these recorded stacks contained continuous areas of intensely stained surface membrane. Such images were excluded from analysis. For all cells this resulted in 8-10 planes analyzed.

Image processing

The sequence of image processing is illustrated in the Online Figure 1. First, image stacks were deconvolved using the Richardson-Lucy algorithm, based on the measured point spread function (PSF), as proposed by Soeller & Cannell [10] (Fug.1 A). The PSF of our confocal system was quantified by measuring the full width half maximum (FWHM) of subresolution fluorescent beads in cristalline solution (Estapor microspheres, 0.1 µm diameter, Merck Eurolab, France), yielding a FWHM of 0.299 µm in X and Y direction and 1.08 µm in Z-direction. Z-spacing of the XY images was too large for a deblurred reconstruction of the T-tubular network in the Z-dimension (Nyquist theorem of signal sampling), and the deconvolution algorithm was applied to each XY plane individually (2D deconvolution).

T-tubule signal within the cell margins was identified against the (cytosolic) background by the Otsu thresholding algorithm [11] coded in IDL (vers. 6.1, ITT Visual Information Solutions, Paris, France), resulting in a binary image (Fig.1 B). The signal threshold was calculated from the intensity histogram as the value resulting in maximal between-class variance of signal and background pixels. To account for changes in global fluorescence signal intensity between cardiomyocytes (i.e., due to variation in dye loading), a signal threshold was calculated for each individual cell from the average of all XY images of that cell. All XY images of the cell were then

thresholded by this value and high frequency noise was filtered by pre-assigned binary erosion.

T-tubule quantification

Sarcolemmal surface membrane was identified in the deconvolved and thresholded XY images as the signal intense margin of the cell and was excluded for all T-tubule signal density measurements (Fig.1 C). T-tubule signal density was then quantified as the number of signal-positive pixels over all pixels within the cell margins.

To compare T-tubular morphology, surface and area of the T-tubular structures in the XY images was determined by contouring (Fig. 1 D).

To quantify T-tubule distribution, XY images were subsequently superimposed with a grid of 5 µm x 5 µm boxes (Fig. 1E). In these images, T-tubule signal density was calculated individually for each box. Results were classified and summarized according to the location of the boxes within the image as follows (Fig.1 E, inset): 'outside' boxes containing only pixels outside the cell, with or without surface membrane (red box); 'inside' boxes containing only pixels inside the cell without sarcolemma and representing the more central regions of the cardiomyocytes (green box); 'partial' boxes containing pixels inside the cell and also sarcolemma, representing subsarcolemmal regions within the cardiomyocytes (blue box) For these partial boxes, only pixels inside the sarcolemma were analyzed. Homogeneity of T-tubule distribution within boxes was further assessed by calculating the variability of T-tubule signal as the percentage error of the signal, i.e. the standard deviation divided by the mean value.

Global $[Ca^{2+}]_i$ and membrane current measurements

Cardiac myocytes were placed in a perfusion chamber on an inverted microscope (Nikon Diaphot). The setup for epifluorescence recording, calibration of the $[Ca^{2+}]_i$-dependent fluorescence and measurement of membrane currents were as described previously [12]. Fluorescence signals were recorded from the entire cell and calibrated after obtaining F_{max} at the end of the experiments [13;14]. I_{CaL} was measured as the nifedipine-sensitive current (20 µmol/L). The Ca^{2+} content of the SR was measured as the integrated inward Na/Ca exchange (NCX) current (I_{NCX}) during caffeine-induced Ca^{2+} release (10 mmol/L, fast application for 10 seconds).

Solutions

Chemicals were purchased from Sigma, fluorescent probes from Invitrogen, Belgium. Pipette solution contained (in mmol/L): K-aspartate 120, KCl 20, HEPES 10, MgATP 5, $MgCl_2$ 0.5, NaCl 10, and K_5-fluo-3 0.05, pH 7.20 with KOH. Tyrode's solution contained (in mmol/L) NaCl 130, KCl 5.4, HEPES 11.8, $MgCl_2$ 0.5, $CaCl_2$ 1.8, and glucose 10, pH 7.40 with NaOH.

Immunofluorescent imaging of RyR and RyR density quantification

Myocytes were fixed and permeabilized by adding an equal volume of 4% paraformaldehyde/0.5% Triton-X (on ice for 15 min). Cells were washed in PBS, incubated with PBS/0.1 mol/L glycine and washed again. The cardiomyocytes were then incubated with PBS with 3% goat serum albumin for 5 min, washed and incubated overnight (4°C) with primary antibody (IgG-anti-RyR, clone 34C, 1:500 in PBS, Affinity BioReagents, Golden, CO, USA). The next day, cardiomyocytes were washed in PBS and incubated with FITC-conjugated secondary antibody (anti-mouse IgG, 1:320 in PBS, Sigma) for 2 hrs at room temperature. Following wash with PBS, cells were used for imaging within 4 hrs. Cardiomyocytes incubated with secondary

antibody only served as negative control and confirmed the absence of staining. Confocal XY image stacks recorded from the RyR-stained cardiomyocytes were deconvolved and thresholded as described in the section Image Processing above. The same algorithms as detailed in the section T-tubule quantification were applied to compare RyR signal density between groups. Mean percentage error of RyR density (as a measure of homogeneity of RyR distribution) was calculated from all boxes of the superimposed grid containing RyR signal.

Immunoblot

Transmural needle biopsies from the ischemic area were taken in situ at the time of sacrifice. Control tissue was obtained from the same area in hearts of CTRL pigs. The tissue was immediately frozen at –80^{o}C. Protein levels were determined in tissue homogenates by immunoblot analysis, essentially as described previously,[15] using commercially available antibodies (NCX Mab clone C2C12, Affinity Bioreagents). The fluorescent signals were quantified on the Storm840 FluorImager with ImageQuant Software (Molecular Dynamics).

Line scan image analysis

Repetitive line scans were stacked yielding line scan images that were analyzed using custom made algorithms coded in IDL. Images were filtered by a running median of five pixels along the spatial and temporal axes. Recordings were segmented according to the onset of the whole-line averaged $[Ca^{2+}]_i$ transients, and 6-10 sequential beats were averaged. The resulting time-averaged line scan image of a $[Ca^{2+}]_i$ transient therefore allowed us to identify cell regions with consistently early or delayed Ca^{2+} release upon depolarization, independent of potential beat-to-beat variability in Ca^{2+} release. All temporal data refer to the onset of the whole-line averaged $[Ca^{2+}]_i$ transient (t_0). Intensity fluorescence values (F) along the scan line were normalized to

the fluorescence intensity at diastole (F_0). For this, scan lines from the last 50 ms (32 lines) of end-diastole (before t_0) were averaged to obtain an averaged F_0 line. Each line of the time-averaged line scan image was then divided by the averaged F_0 line. F_{50} was defined as the half-maximum of the normalized overall peak $[Ca^{2+}]_i$-dependent fluorescence and served as threshold to discriminate local Ca^{2+} release as previously described [6]. Sections of the line where F did not reach F_{50} within 200 ms were excluded from analysis.

Statistics

Data are shown as mean±S.E.M. and were compared using Student's t-test or two-way ANOVA; Fisher's least-significant difference test was performed when significant overall effects were detected. $P< 0.05$ was considered significant.

Results

T-tubule properties

Contouring of the T-tubules yielded a value of the contour/surface area, approximating in 2D a surface:volume ratio. Swollen T-tubules are expected to have a larger surface:volume ratio. The data were not different for MI (7.70±0.13 vs. 0.84±0.19 in CTRL; ncells = 35 and 38 respectively).

Separate analysis of T-tubule density in the subsarcolemmal region and of the interior of the cell was obtained by comparing T-tubule signal density in 'partial', versus 'inside' boxes. This analysis showed that the density was higher in the subsarcolemmal regions compared to the central regions, for both groups, without difference in the subsarcolemmal density between groups (17±8 vs. and 18±8% for MI and CTRL resp). In the central regions however, differences were marked (10±7% in MI vs. 15±9 in CTRL).

Analysis of 'sparks' in the line scan image

A reduction in couplon size, i.e. in the number of L-type Ca^{2+} channels per couplon, would in itself lead to dyssynchrony, as shown by Bridge and co-workers[16;17]. A smaller couplon size can be revealed by a broader distribution of the latency to release or a reduced opening probability seen as spark incidence for a given latency. Our experimental conditions are not comparable to those studies and less optimal for this type of spark analysis, because of the low Ca^{2+} buffering allowing free Ca^{2+} diffusion, and because we record at +10 mV with a very high probability of release. In addition the number of recordings per site did not exceed 10 pulses. Within these limitations, we nevertheless performed additional analysis of the data. First we defined 'spark' sites based on the highest amplitude of the local transient in each cell (n=41 in CTRL and n=35 in MI). After automated iterative segmentation, 407 sites in CTRL myocytes and 340 sites in MI myocytes were categorized as 'sparks' for further analysis (3 detected spark sites in CTRL and 10 in MI, respectively, were excluded due to motion artefacts). Peak amplitudes of the selected sparks were not different between CTRL and MI (4.54±0.23 vs. 4.60±0.36 F/F_0). 'Probability of spark', defined as the probability of having F> F50 within 50 ms was 1 for all sparks detected in CTRL and for the large majority (96.2%) of sparks in MI.

Next we determined the latency of release, as the time to half maximum, TF50, at each site for an average of 9 consecutive transients. We calculated the histogram of mean spark latencies of individual sparks, pooled all data and fitted an exponential to the decline of the frequency distribution (Online Figure 2). There is no obvious difference in the decay constant in MI, but the graph shows that there are data points at long latencies that are poorly described by the fitting procedure. We therefore did

an additional analysis of the longer latencies. In MI, more of the identified sparks had a mean latency > 20 ms (18.9% in MI vs. 11.7% in CTRL, P< 0.05 chi square).

Next we examined the variability of spark latency at individual spark sites. The variation of spark latencies was higher in MI vs. CTRL (3.4±0.1 vs. 2.9±0.1 ms, P< 0.01).

This analysis would indicate that MI cells are more likely to have couplons with fewer LCC, taking the presence of a higher variability as a sufficient argument. What we are lacking however are the data for P_{spark} as a function of latency which should distinguish groups of sparks with the same mean latency but different P_{spark} because of different numbers of LCC present. Further experiments with a larger number of recordings per site, smaller depolarizing steps and better resolved sparks are needed to confirm this analysis.

References

1. Weidemann F, Dommke C, Bijnens B, Claus P, D'hooge J, Mertens P, Verbeken E, Maes A, Van de Werf F, De Scheerder I, Sutherland GR. Defining the transmurality of a chronic myocardial infarction by ultrasonic strain-rate imaging: implications for identifying intramural viability: an experimental study. *Circulation*. 2003;107:883-888.

2. Rademakers F, Van de WF, Mortelmans L, Marchal G, Bogaert J. Evolution of regional performance after an acute anterior myocardial infarction in humans using magnetic resonance tagging. *J Physiol*. 2003;546:777-787.

3. Cerqueira MD, Weissman NJ, Dilsizian V, Jacobs AK, Kaul S, Laskey WK, Pennell DJ, Rumberger JA, Ryan T, Verani MS. Standardized myocardial segmentation and nomenclature for tomographic imaging of the heart: a statement for healthcare professionals from the Cardiac Imaging Committee of the Council on Clinical Cardiology of the American Heart Association. *Circulation*. 2002;105:539-542.

4. Kim RJ, Fieno DS, Parrish TB, Harris K, Chen EL, Simonetti O, Bundy J, Finn JP, Klocke FJ, Judd RM. Relationship of MRI delayed contrast enhancement to irreversible injury, infarct age, and contractile function. *Circulation*. 1999;100:1992-2002.

5. Bito V, Heinzel FR, Weidemann F, Dommke C, van der Velden J, Verbeken E, Claus P, Bijnens B, De Scheerder I, Stienen GJ, Sutherland GR, Sipido KR. Cellular mechanisms of contractile dysfunction in hibernating myocardium. *Circ Res*. 2004;94:794-801.

6. Heinzel FR, Bito V, Volders PG, Antoons G, Mubagwa K, Sipido KR. Spatial and temporal inhomogeneities during Ca2+ release from the sarcoplasmic reticulum in pig ventricular myocytes. *Circ Res*. 2002;91:1023-1030.

7. Louch WE, Bito V, Heinzel FR, Macianskiene R, Vanhaecke J, Flameng W, Mubagwa K, Sipido KR. Reduced synchrony of Ca^{2+} release with loss of T-tubules - a comparison to human failing cardiac myocytes. *Cardiovasc Res*. 2004;62:63-73.

8. Loughrey CM, Seidler T, Miller SL, Prestle J, MacEachern KE, Reynolds DF, Hasenfuss G, Smith GL. Over-expression of FK506-binding protein FKBP12.6 alters excitation-contraction coupling in adult rabbit cardiomyocytes. *J Physiol*. 2004;556:919-934.

9. Cheng H, Song LS, Shirokova N, Gonzalez A, Lakatta EG, Rios E, Stern MD. Amplitude distribution of calcium sparks in confocal images: theory and studies with an automatic detection method. *Biophys J*. 1999;76:606-617.

10. Soeller C, Cannell MB. Examination of the transverse tubular system in living cardiac rat myocytes by 2-photon microscopy and digital image-processing techniques. *Circ Res*. 1999;84:266-275.

11. Otsu N. A thresholding selection method from gray-level histogram. *IEEE Transactions on Systems, Man, and Cybernetics*. 1979;9:62-66.

12. Antoons G, Mubagwa K, Nevelsteen I, Sipido KR. Mechanisms underlying the frequency dependence of contraction and $[Ca^{2+}]_i$ transients in mouse ventricular myocytes. *J Physiol (Lond)*. 2002;543:889-898.

13. Antoons G, Ver Heyen M, Raeymaekers L, Vangheluwe P, Wuytack F, Sipido KR. Calcium uptake by the sarcoplasmic reticulum in ventricular myocytes of the SERCA2a$^{-/-}$ mouse is impaired at higher Ca^{2+} loads only. *Circ Res*. 2003;92:881-887.

14. Trafford AW, Diaz ME, Eisner DA. A novel, rapid and reversible method to measure Ca buffering and time-course of total sarcoplasmic reticulum Ca content in cardiac ventricular myocytes. *Pflugers Arch*. 1999;437:501-503.

15. Harrer JM, Kiss E, Kranias EG. Application of the immunoblot technique for quantitation of protein levels in cardiac homogenates. *Biotechniques*. 1995;18:995-998.

16. Inoue M, Bridge JH. Ca2+ sparks in rabbit ventricular myocytes evoked by action potentials: involvement of clusters of L-type Ca2+ channels. *Circ Res*. 2003;92:532-538.

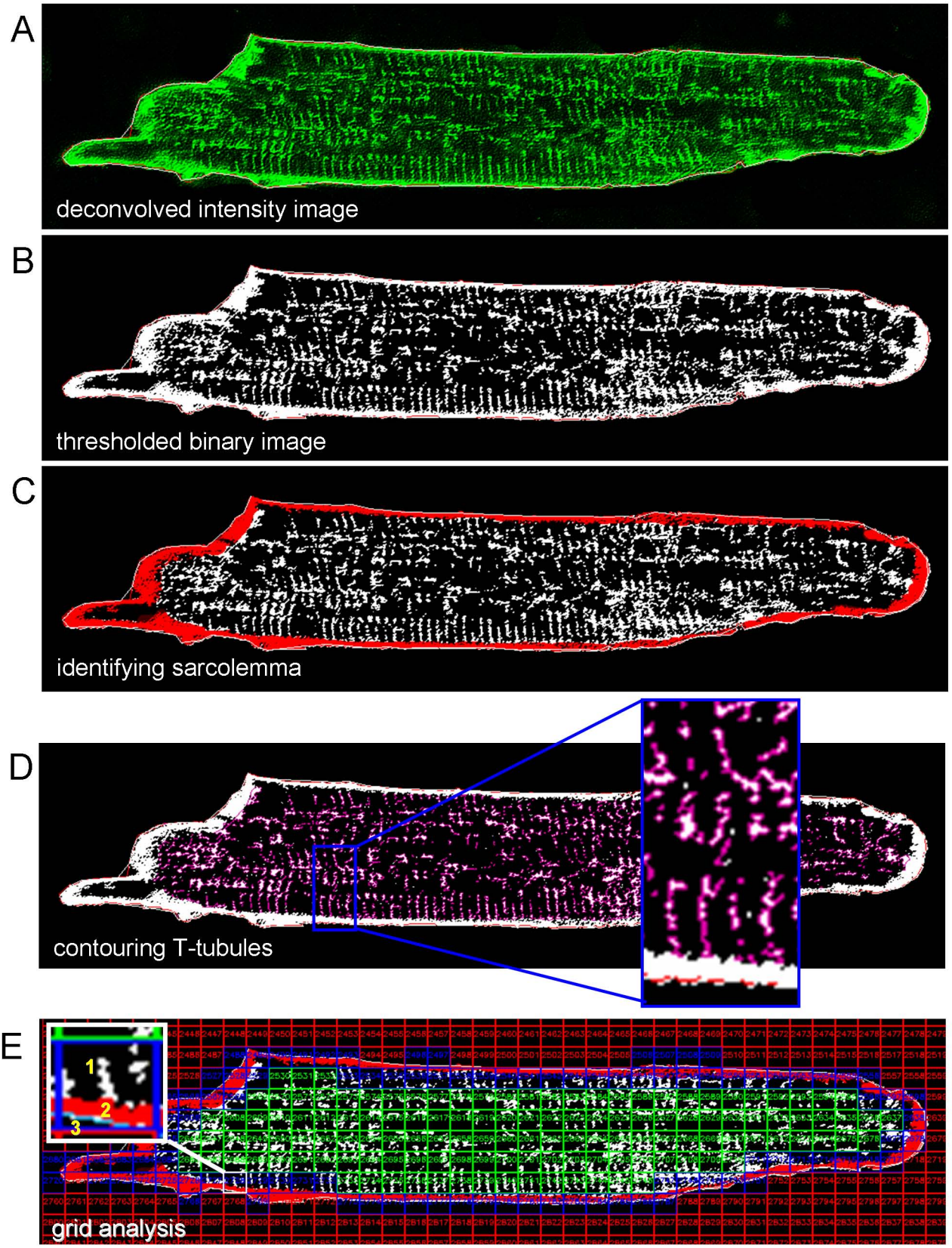

red= box completely outside cell, **blue**= box partially inside cell, **green**= box completely inside cell
Blue boxes contain different pixel classes: 1= inside cell, 2= sarcolemma, 3= extracellular.
T-tubule signal density for each box is calculated from the class 1 pixels, i.e inside the cell.

Online Figure 1

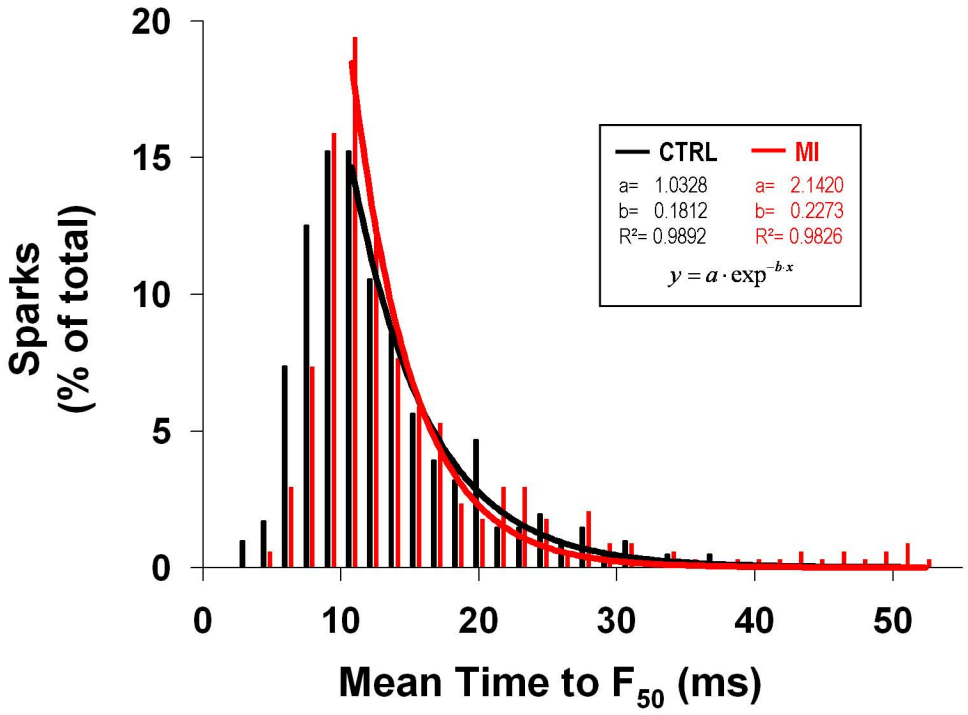

Online Figure 2

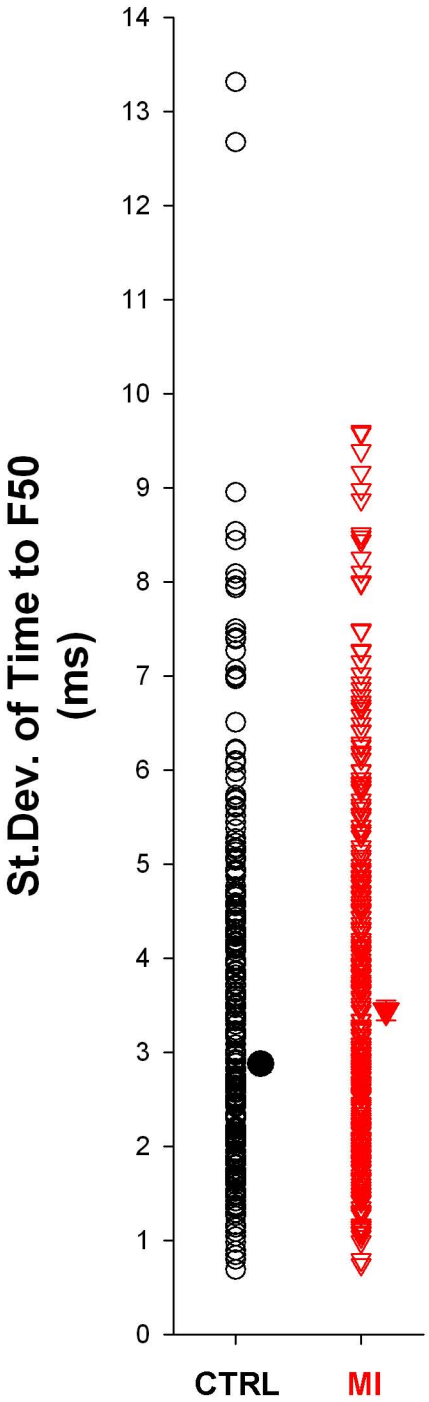

Online Figure 3